Expanded View Figures

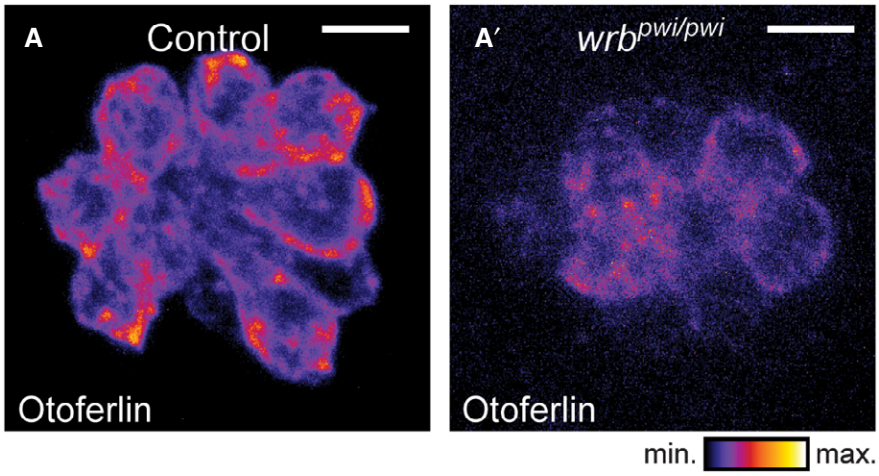

Figure EV1. Wrb dependence of otoferlin expression in HCs of zebrafish neuromasts (related to Fig 1).

A, A′ Immunostaining of otoferlin in 5-dpf zebrafish neuromasts, presented in an intensity-coded LUT to illustrate the reduced otoferlin signal in *wrb*$^{pwi/pwi}$ compared to control fish. Scale bar: 5 μm.

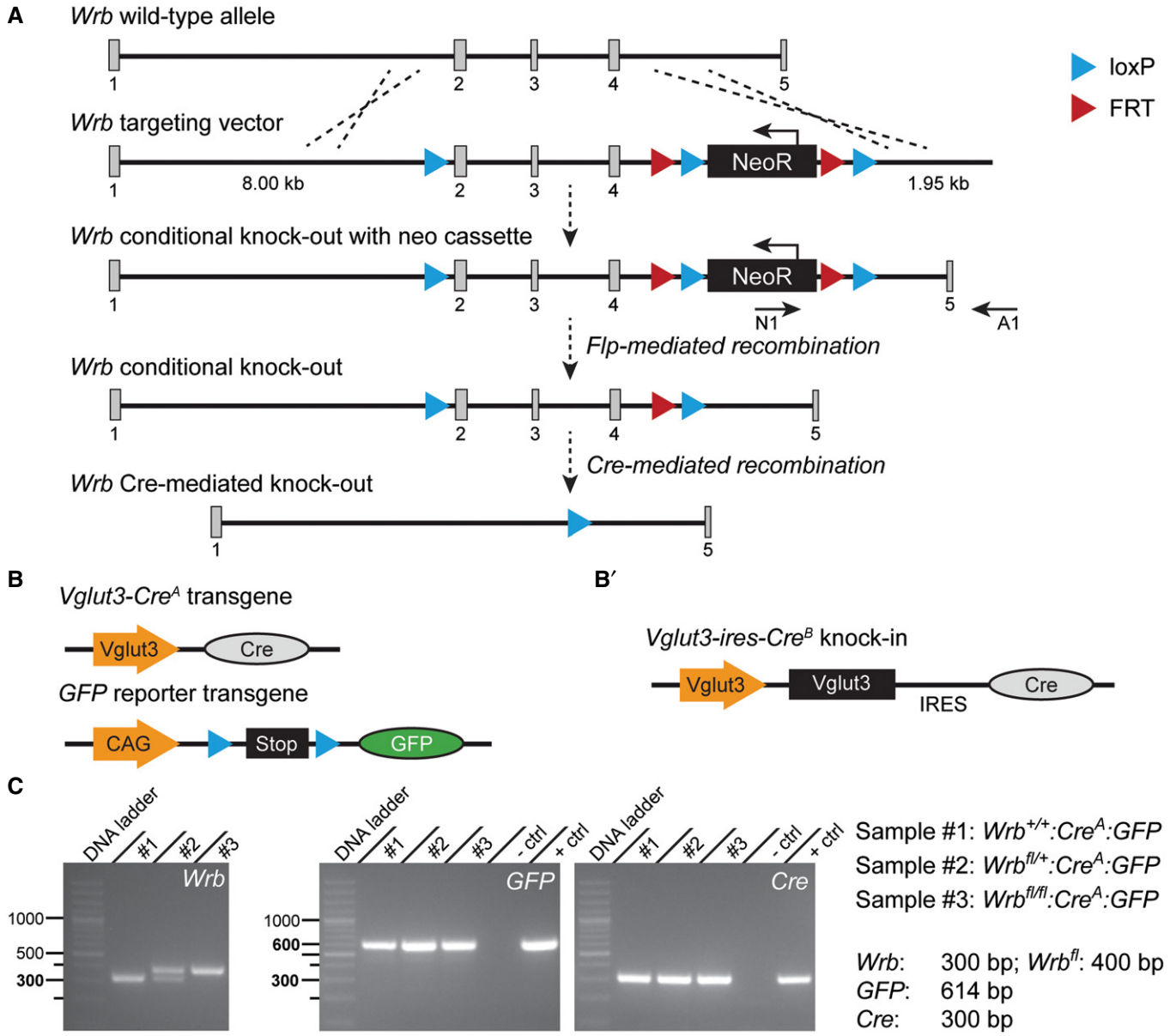

Figure EV2. Strategy for conditional inactivation of the *Wrb* gene in mice (related to Figs 3–7).

A The wild-type allele with five exons is shown on top, below then the targeting vector, the targeted allele with the neomycin cassette, which served as selection marker of ES cells (the neomycin resistance gene is removed in ES cells through the activity of flipase-mediated recombination acting on the FRT sites), followed by the targeted conditional knockout allele after Flp recombination and lastly the *Wrb* allele after homologous Cre recombination and excision of exons 2–4.

B Maps of the Cre-expressing transgene under the *Vglut3* gene promoter and of the GFP reporter transgene containing a stop cassette flanked by loxP sites. Cre-directed homologous recombination at loxP sites of *Wrb* conditional knockout and at GFP reporter transgene results in *Wrb* Cre-mediated knockout alongside removal of the stop cassette before GFP and thus GFP expression.

B′ Map of the knock-in transgene where the coding sequence of Cre is inserted at the end of the *Vglut3* gene locus following an internal ribosomal entry site (IRES) segment.

C PCR genotyping results. Tail DNA from three mouse littermates was used to demonstrate the Cre-mediated expression of Wrb in the three genotypes. In the conditional knockout mouse (sample #3), the length of the *Wrb* allele is bigger than in the wild-type mouse (sample #1), due to the extra two loxP and one FRT sites inserted in the gene. Sample #2 is from a heterozygous animal, which expresses only one *Wrb* conditional allele. PCR from this sample demonstrates 2 bands, one of the wild-type allele and the other of the transgene. The expression of GFP and Cre is confirmed in all three genotypes. Brain tissue was used as a positive control.

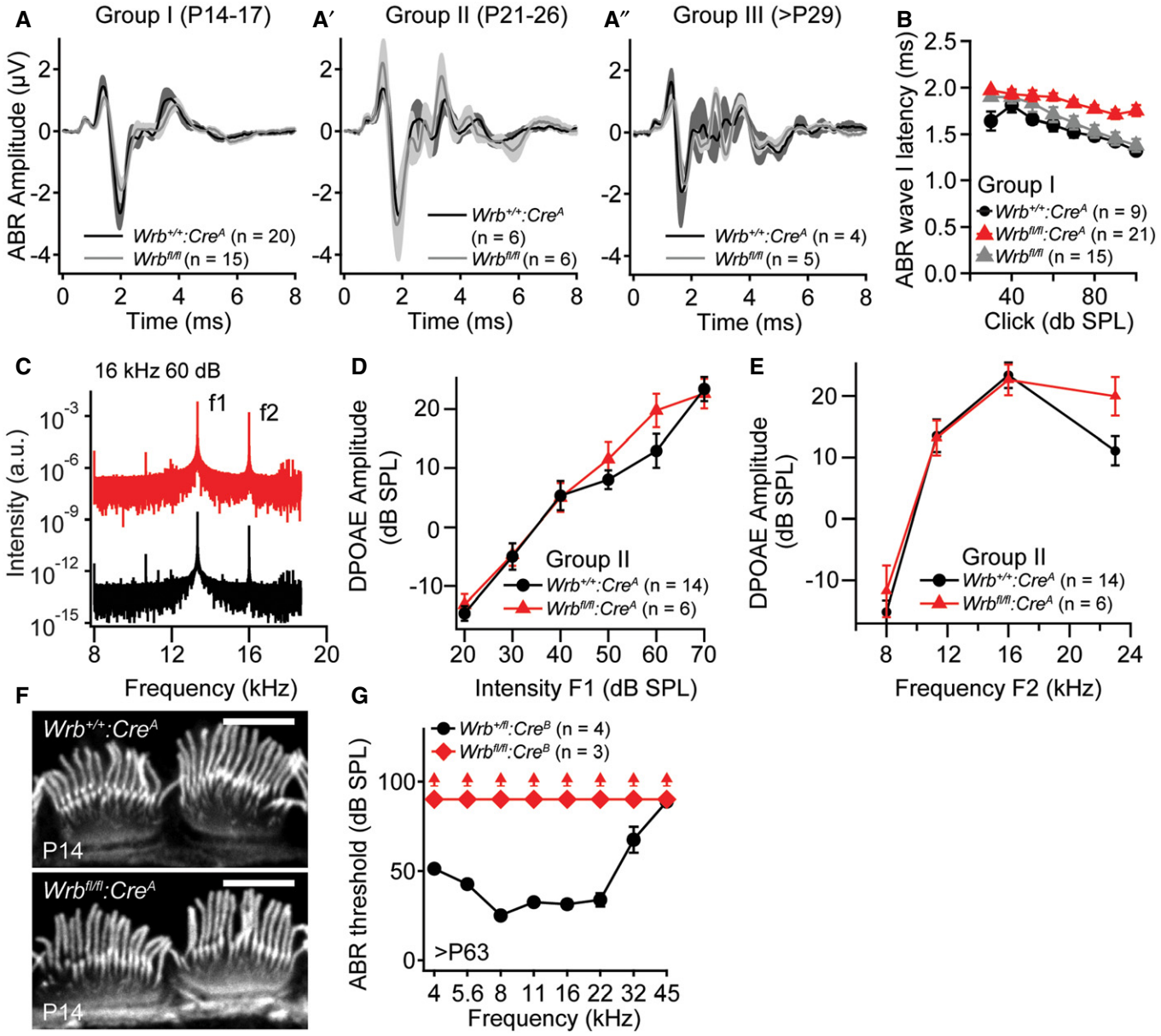

Figure EV3. Wrb disruption in hair cells causes a synaptopathic hearing impairment (related to Figs 3 and 7).

A–A″ ABR wave I amplitudes of $Wrb^{+/+}$:Cre^{A} and $Wrb^{fl/fl}$ control animals of groups I-III are normal in transgenic animals lacking Cre expression.

B ABR latencies of group I animals are increased in $Wrb^{fl/fl}$:Cre^{A} when compared to $Wrb^{+/+}$:Cre^{A} and $Wrb^{fl/fl}$ control animals.

C Representative example frequency spectra of DPOAEs at 10.67 kHz measured from $Wrb^{fl/fl}$:Cre^{A} and $Wrb^{+/+}$:Cre^{A} mice to primary tones of 13.3 (70 dB) and 16 kHz (60 dB).

D, E No statistically significant differences in (D) mean DPOAE amplitudes at increasing sound intensities in $Wrb^{fl/fl}$:Cre^{A} and $Wrb^{+/+}$:Cre^{A} (exemplary at 16 kHz) or (E) across the entire measured frequency range (at intensities of 70 dB (f1) and 60 dB (f2)) could be observed, indicating unaltered cochlear amplification and OHC function in the mutants.

F IHC hair bundles appear normal in $Wrb^{fl/fl}$:Cre^{A} animals as assessed with fluorophore-conjugated phalloidin stainings at P14. Scale bar: 5 μm.

G Lack of ABR in > P63 $Wrb^{fl/fl}$:Cre^{B} mice across the entire frequency range. Upwards pointing arrowheads indicate thresholds exceeding the maximum speaker output of 90 dB.

Data information: All data are represented as mean ± SEM.

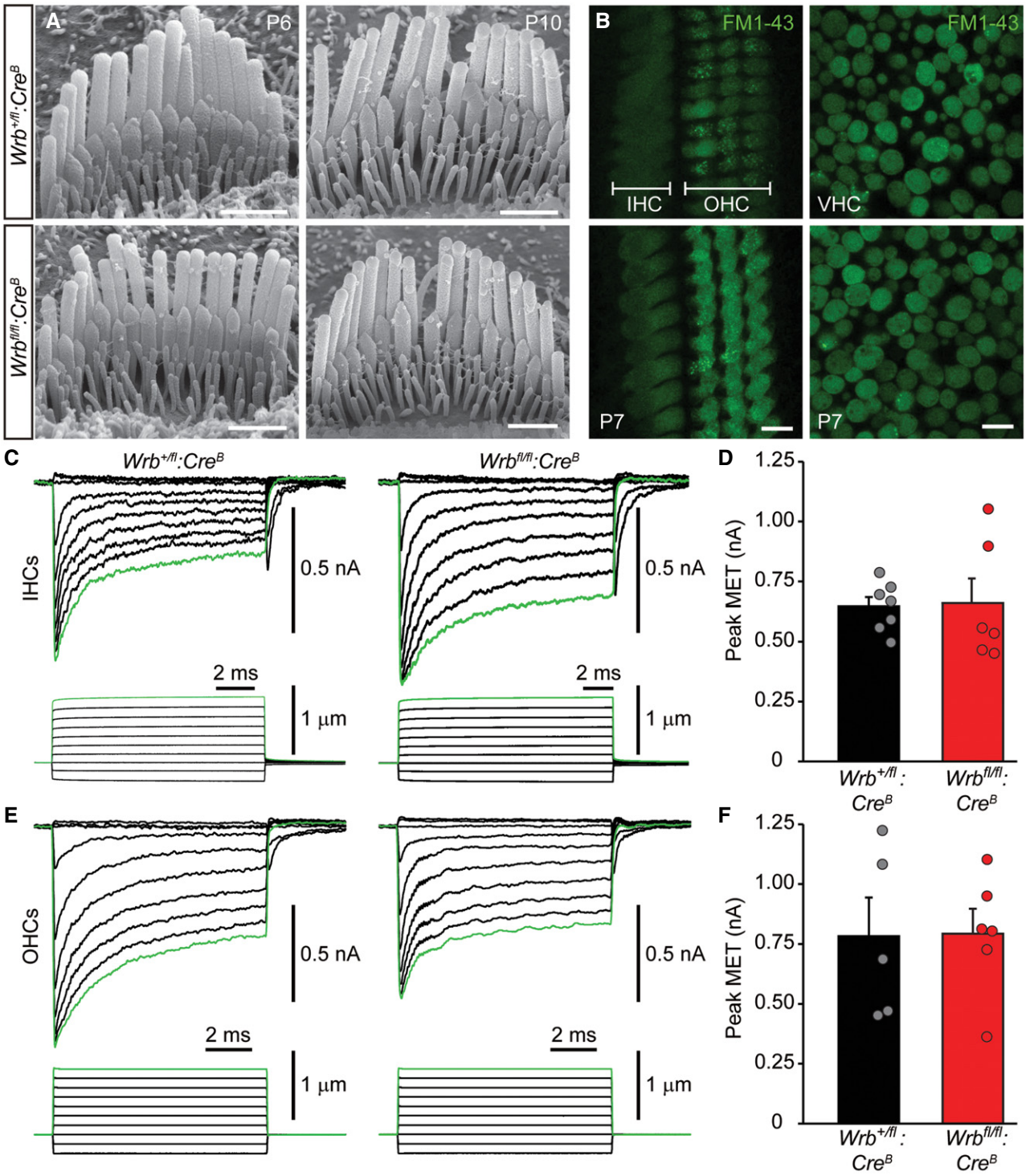

Figure EV4. Wrb-deficient IHCs show normal hair bundle development, maintenance, and MET function (related to Figs 3 and 7).

A Scanning electron micrographs of P6 and P10 IHCs of *Wrb*$^{+/fl}$:*Cre*^{B} (top) and *Wrb*$^{fl/fl}$:*Cre*^{B} (bottom) mice. No obvious deficit in bundle development was detected in Wrb-deficient mice. Scale bars: 1 μm.

B FM1-43 uptake by P7 auditory (IHC and OHC) and vestibular hair cells shows no obvious difference in fluorescence levels between *Wrb*$^{+/fl}$:*Cre*^{B} (top) and *Wrb*$^{fl/fl}$:*Cre*^{B} (bottom) mice. Scale bars: 10 μm.

C–F Representative MET responses to a family of stepwise deflections of the hair cell bundle for (C) IHCs and (E) OHCs in *Wrb*$^{+/fl}$:*Cre*^{B} (left) and *Wrb*$^{fl/fl}$:*Cre*^{B} (right) mice. Means ± SEM of the MET currents are presented in (D) for IHCs and (F) for OHCs, with individual values for each cell shown as circles. No statistically significant differences were found in peak MET current amplitude in Wrb-deficient IHCs or OHCs.

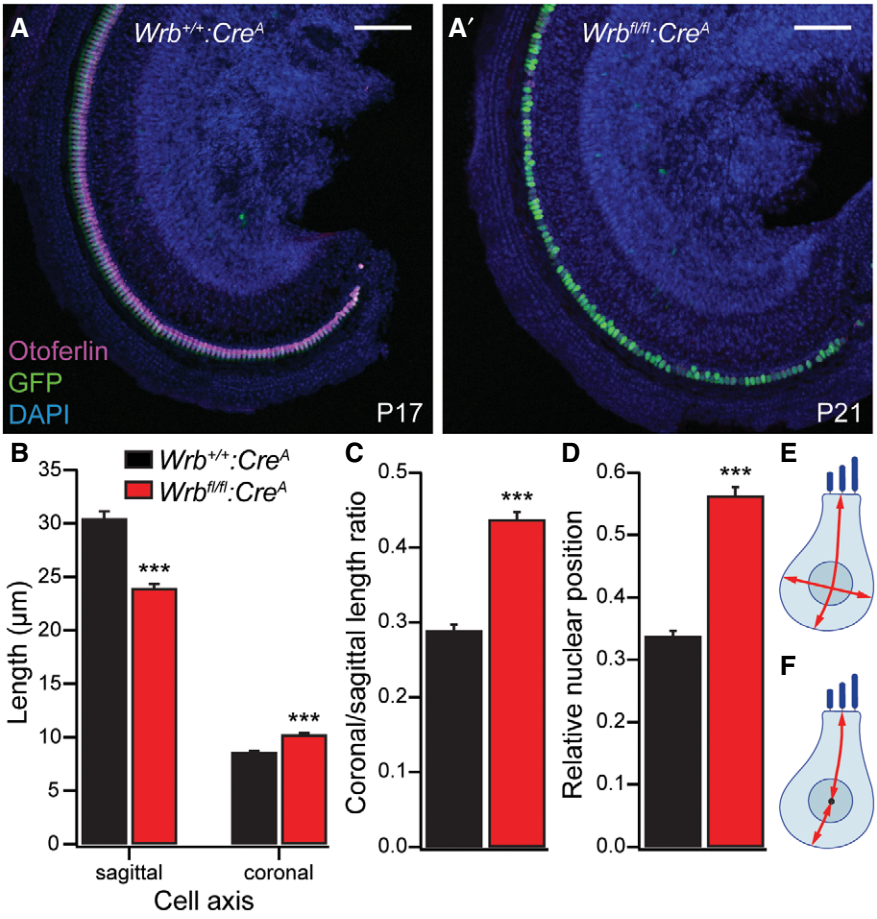

Figure EV5. Wrb disruption affects IHC morphology.

A, A′ Representative low-magnification (10×) confocal projections of apical turn whole-mount organs of Corti from $Wrb^{+/+}$:Cre^{A} P17 (A, same specimen as shown in Appendix Fig S4) and $Wrb^{fl/fl}$:Cre^{A} P21 (A′) animals immunolabeled for GFP (green, reporting Cre recombination), otoferlin (magenta, labeling IHCs), and DAPI (blue, labeling all cell nuclei). Scale bar: 100 µm. Note that Wrb deficiency does not lead to a dramatic loss of IHCs, but a change in IHC morphology. Cell shape and nuclear position were analyzed in images taken with higher magnification (63×, see Fig 4).

B, C Wrb-deficient IHCs (P18–21) show significantly decreased sagittal, but increased coronal extent (Wilcoxon rank test, $***P < 0.001$), resulting in an increased ratio of these two measurements (Wilcoxon rank test, $***P < 10^{-15}$, $n = 46$ and 67 Wrb-deficient and control IHCs from four and six P18–21 $Wrb^{+/+}$:Cre^{A} and $Wrb^{fl/fl}$:Cre^{A} animals, respectively). Custom-written MATLAB routines were used for the analysis. Data are represented as means ± SEM.

D Nuclear position is altered in $Wrb^{fl/fl}$:Cre^{A} animals, where nuclei are located closer to the cell base as compared to controls. The relative distance from the apical plane of a cell is given. Data are represented as means ± SEM.

E, F Schematic drawings illustrating the analysis performed in (B–D).